Available online at www.sciencedirect.com
SCIENCE DIRECT®
Icarus 169 (2004) 80–97
ICARUS
www.elsevier.com/locate/icarus

Mapping of the Culann–Tohil region of Io from Galileo imaging data

David A. Williams,[a,*] Paul M. Schenk,[b] Jeffrey M. Moore,[c] Laszlo P. Keszthelyi,[d,e] Elizabeth P. Turtle,[e,f] Windy L. Jaeger,[e] Jani Radebaugh,[e] Moses P. Milazzo,[e] Rosaly M.C. Lopes,[g] and Ronald Greeley [a]

[a] *Department of Geological Sciences, Arizona State University, Bateman Physical Sciences Building F506B, Tempe, AZ 85287-1404, USA*
[b] *USRA Center for Advanced Space Studies (CASS), Lunar and Planetary Institute, 3600 Bay Area Boulevard, Houston, TX 77058, USA*
[c] *Space Sciences Division, NASA Ames Research Center, MS 245-3, Moffett Field, CA 94035, USA*
[d] *Astrogeology Team, US Geological Survey, 2255 N. Gemini Drive, Flagstaff, AZ 86001, USA*
[e] *Lunar and Planetary Laboratory, University of Arizona, 1629 E. University Boulevard Tucson, AZ 85721, USA*
[f] *Planetary Science Institute, 1700 E. Ft. Lowell, Suite 106, Tucson, AZ, USA*
[g] *NASA Jet Propulsion Laboratory, California Institute of Technology, MS 183-601, 4800 Oak Grove Drive, Pasadena, CA 91109, USA*

Received 14 March 2003; revised 7 August 2003

Abstract

We have used Galileo spacecraft data to produce a geomorphologic map of the Culann–Tohil region of Io's antijovian hemisphere. This region includes a newly discovered shield volcano, Tsũi Goab Tholus and a neighboring bright flow field, Tsũi Goab Fluctus, the active Culann Patera and the enigmatic Tohil Mons-Radegast Patera–Tohil Patera complex. Analysis of Voyager global color and Galileo Solid-State Imaging (SSI) high-resolution, regional (50–330 m/pixel), and global color (1.4 km/pixel) images, along with available Galileo Near-Infrared Mapping Spectrometer (NIMS) data, suggests that 16 distinct geologic units can be defined and characterized in this region, including 5 types of diffuse deposits. Tsũi Goab Fluctus is the center of a low-temperature hotspot detected by NIMS late during the Galileo mission, and could represent the best case for active effusive sulfur volcanism detected by Galileo. The Culann volcanic center has produced a range of explosive and effusive deposits, including an outer yellowish ring of enhanced sulfur dioxide (SO_2), an inner red ring of SO_2 with short-chain sulfur (S_3–S_4) contaminants, and two irregular green diffuse deposits (one in Tohil Patera) apparently produced by the interaction of dark, silicate lava flows with sulfurous contaminants ballistically-emplaced from Culann's eruption plume(s). Fresh and red-mantled dark lava flows west of the Culann vent can be contrasted with unusual red–brown flows east of the vent. These red–brown flows have a distinct color that is suggestive of a compositional difference, although whether this is due to surface alteration or distinct lava compositions cannot be determined. The main massif of Tohil Mons is covered with ridges and grooves, defining a unit of tectonically disrupted crustal materials. Tohil Mons also contains a younger unit of mottled crustal materials that were displaced by mass wasting processes. Neighboring Radegast Patera contains a NIMS hotspot and a young lava lake of dark silicate flows, whereas the southwest portion of Tohil Patera contains white flow-like units, perhaps consisting of 'ponds' of effusively emplaced SO_2. From 0°–15° S the hummocky bright plains unit away from volcanic centers contains scarps, grooves, pits, graben, and channel-like features, some of which have been modified by erosion. Although the most active volcanic centers appear to be found in structural lows (as indicated by mapping of scarps), DEMs derived from stereo images show that, with the exception of Tohil Mons, there is less than 1 km of relief in the Culann–Tohil region. There is no discernable correlation between centers of active volcanism and topography.

Keywords: Satellites of Jupiter; Io; Geological processes; Volcanism; Surfaces (satellite)

1. Introduction

After almost 14 years in space, NASA's Galileo spacecraft completed remote sensing observations in January 2002 and entered a ballistic trajectory to impact into Jupiter on September 21, 2003. As part of the ongoing analysis of data returned by the Galileo spacecraft of Jupiter's volcanic moon Io (see, e.g., McEwen et al., 1998a, 2000; Keszthelyi et al., 2001; Turtle et al., 2004; McEwen, 2002), we are producing a series of regional geomorphologic maps of several portions of the well-imaged antijovian hemisphere to

* Corresponding author.
E-mail address: david.williams@asu.edu (D.A. Williams).

0019-1035/$ – see front matter
doi:10.1016/j.icarus.2003.08.024

complement the Voyager-era maps of the subjovian hemisphere (Moore, 1987; Greeley et al., 1988; Schaber et al., 1989; Whitford-Stark et al., 1991; Crown et al., 1992). Our first map focused on the Chaac–Camaxtli region (Williams et al., 2002), which contains a wide range of volcanic structures (paterae), flow fields and extensive plains. In this paper we present a map of the Culann–Tohil region, which contains the active volcano Culann Patera and the enigmatic mountain-volcano complex: Tohil Mons, Radegast Patera, and Tohil Patera. Culann Patera is at the center of a dynamic volcanic complex (see cover of Science, 288, No. 5469, 19 May 2000) that has produced diverse volcanic deposits, and Tohil is a well-studied example of Io's unusual mountains, many of which are found in close proximity to one or more paterae (e.g., Turtle et al., 2001; Jaeger et al., 2003). As in our previous paper, we used various image mosaics obtained by the Galileo Solid State Imaging (SSI) experiment (combined with lower resolution SSI color data), along with Near Infrared Mapping Spectrometer (NIMS) multispectral data, which provide temperature estimates and compositional information, to produce a geomorphologic map of this region. Where imaging coverage in this region allowed, Galileo images were also used to create Digital Elevation Models (DEMs) to investigate topographic relationships. From these data, we infer the history of volcanic activity in this region, and compare this region with the previously mapped Chaac–Camaxtli region (Williams et al., 2002).

2. Background

2.1. Approach

A review of previous geologic mapping of Io using Voyager images, along with a summary of current interpretations of Io color and age relationships were given in our previous mapping paper on the Chaac–Camaxtli region (Williams et al., 2002). Our goals in mapping the Culann–Tohil region include:

(1) deciphering the range of volcanic activity at Culann Patera as indicated by its multicolored appearance,
(2) understanding the geologic evolution of Tohil Mons and its relationship to nearby paterae, and
(3) comparing the geology of this region to that in our map of the Chaac–Camaxtli region to further understand how the regional geologic relationships are related to broader questions about Io's nature and evolution.

For example, are there differences in volcanic vent morphologies, tectonic styles, or eruption products between these two regions of the antijovian hemisphere?

We follow the established techniques for planetary mapping (e.g., Shoemaker and Hackman, 1962; Wilhelms, 1972, 1990; Tanaka et al., 1994), in order to identify the variety and sequence of volcanic materials in this region and how they have modified the surface. Strictly speaking, our maps are "geomorphologic maps" rather than "geologic maps" in the sense that terrestrial geologists define them, as all of our mapping is based on morphologic, albedo, color or spectral variations in remote sensing data, and we do not have any direct observations of lithologies or rock ages. Experience from terrestrial field mapping demonstrates that remote sensing-based, nonground-truthed, geologic mapping is able to provide accurate three-dimensional distributions of rock types and their age relationships only under ideal circumstances. Nevertheless, traditional planetary geologic mapping remains a useful tool to organize observations and present results until ground truth can be obtained (Wilhelms, 1990; Moore and Wilhelms, 2001).

2.2. Galileo SSI imaging of the Culann–Tohil region

Figures 1a and 1b contain the best Voyager and Galileo views (respectively) of the Culann–Tohil region, including the approved names for geologic features in this region (see Table 1). This region is located in the leading quadrant of Io's antijovian hemisphere between 5° N–42° S and 155°–170° W, and is roughly bounded in the north by Michabo Patera (to the west of Prometheus) in Colchis Regio, and bounded in the south by Mycenae Regio. This region of Io was poorly imaged by the Voyager spacecraft, with resolutions between 5–20 km/pixel (Smith et al., 1979a, 1979b). No geological studies of this region were done using Voyager data, except for the mapping of ambiguous dark spots as "Patera Floor Material" in the global geologic map of Crown et al. (1992). These spots are now known to be associated with the volcanoes Michabo Patera, Tsũi Goab Fluctus and Tsũi Goab[1] Tholus, Culann Patera, Wabasso Patera, Tohil Patera and Radegast Patera. Crown et al. (1992) also mapped several of the Culann lava flows as a unit of "Lobate Material."

The primary image product (Fig. 1b) used for our mapping is the 6-frame mosaic of the Culann–Tohil region (observation I32TERMIN01, 330 m/pixel; see also Turtle et al., 2004) obtained during the Galileo I32 flyby (October 2001), merged with the C21 low-phase angle (4°), low-resolution (1.4 km/pixel) color data (for a list of Galileo orbit designations, see Table 2). The near-terminator observation captured the geologic features in this region at a low-sun angle (incidence angle = 81°), and thus provides a good view of local topography. Previously obtained mosaics of Culann (observation I25CULANN01, 205 m/pixel; McEwen et al., 2000; Keszthelyi et al., 2001) and Tohil (I27TOHIL01, 165 m/pixel; Turtle et al., 2001) merged with orbit C21 color data (Fig. 2) were also used in this study to help define and characterize the geologic units in this region. The orbit

[1] The Khoi-Khoi (Hottentot) god of rain and thunder has the full name Tsũi Goab, which has also been spelled as Tsuni Goam (Werner, 1964). Hereafter in this paper, volcanic features with this name will use the name Tsũi Goab.

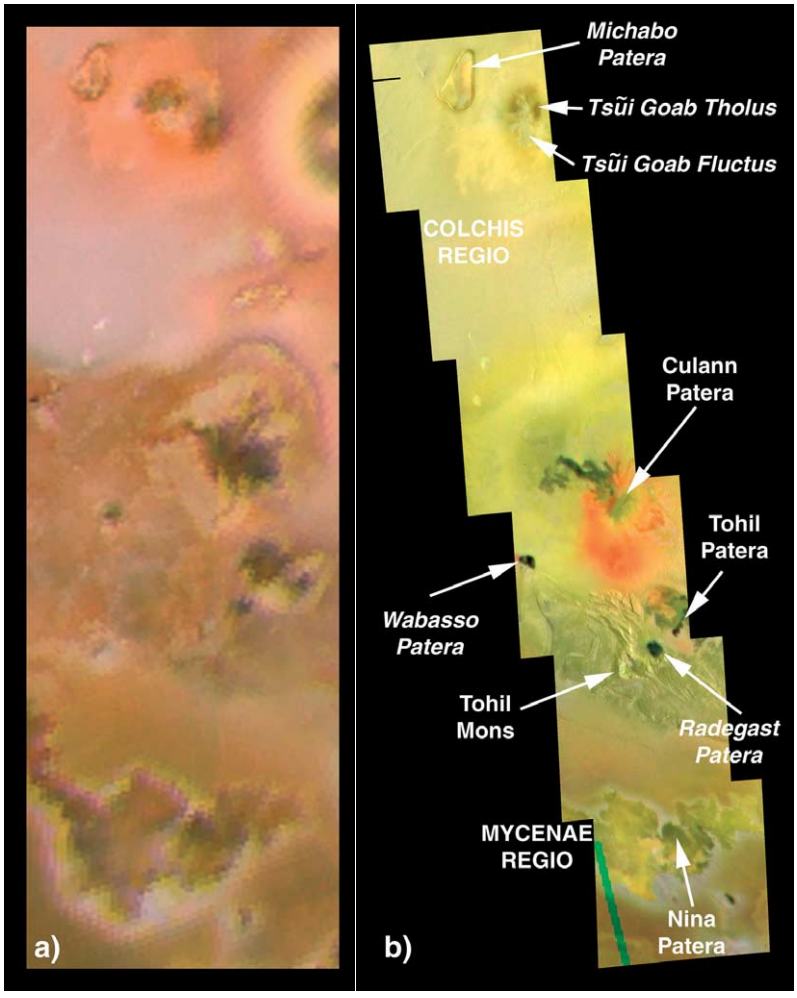

Fig. 1. (a) Best Voyager coverage of the Culann–Tohil region, with resolution between 5–20 km/pixel. Extracted from NASA Planetary Photojournal Catalog Image #PIA00319. (b) Galileo color mosaic of the Culann–Tohil region. This image combines the 6-frame regional mosaic I32ISTERMIN01 (330 m/pixel) with the lower-resolution color mosaic C21ISCOLOR01 (1.4 km/pixel, phase angle = 4°). The I32 mosaic is an orthographic projection, centered on the sub-spacecraft point (3.5° S, 130.6° W), and was obtained at a low-sun angle (incidence angle = 81°) near the terminator, with illumination coming from the east. Non-horizontal faces are illuminated, enabling detection of topographic features. Galileo image processing by Moses Milazzo, University of Arizona.

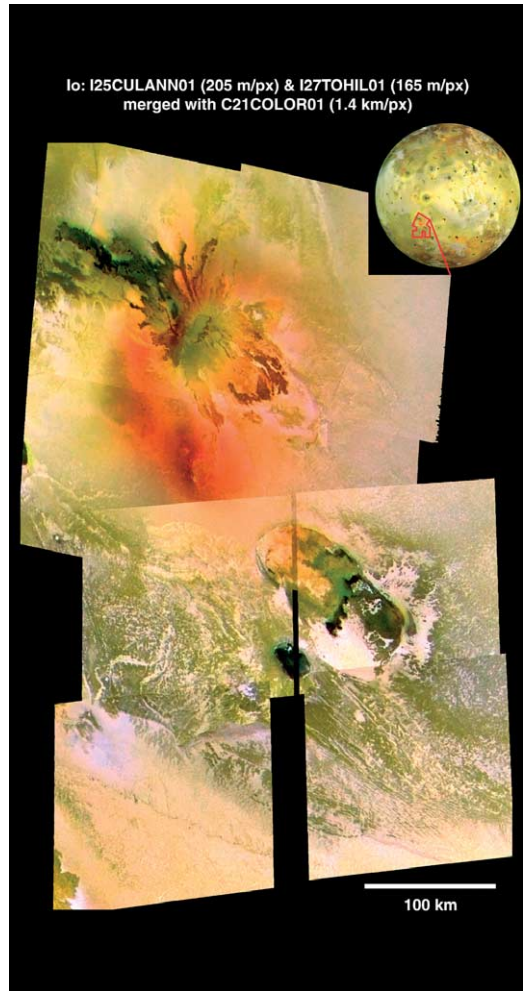

Fig. 2. Galileo color mosaic of the central Culann–Tohil region, including Culann Patera, Tohil Mons, Tohil Patera, and Radegast Patera. This image combines the 4-frame I25 Culann mosaic I25ISCULAN01 (205 m/pixel) and the 4-frame I27 Tohil mosaic I27ISTOHIL01 (165 m/pixel) with the lower-resolution color mosaic C21ISCOLOR01 (1.4 km/pixel, phase angle = 4°). This composite mosaic is an orthographic projection, centered on the sub-spacecraft point (25.5° S, 160° W), and was obtained at a high-sun angle, with illumination coming from the east. Image processing by Moses Milazzo, University of Arizona.

I32 encounter also included a very high resolution, low-sun mosaic of parts of Tohil Mons, Radegast Patera, and Tohil Patera (observation I32TOHIL01, ∼ 50 m/pixel; Turtle et al., 2004) (Fig. 3), which was used to aid in morphological characterizations of some units.

Topographic data for the map area are derived from two techniques. Semi-controlled topography was derived from analysis of C21–I24 regional stereo image coverage at ∼ 1.4 km/pixel horizontal resolution. The derived DEM (method described in Schenk and Bulmer (1998) and Schenk and Wilson, in preparation) has a vertical precision of ∼ 550 m, but is somewhat compromised by radiation damage to the images, which gives the DEM a speckle similar to that seen in Magellan radar images. Nonetheless, areas of high contrast are well represented in the DEM. Additional high resolution DEM data of Tohil Mons were derived from I24–I27 stereo imaging at 150 m/pixel horizontal resolution (Fig. 4). These data have a vertical precision of ∼ 80 m. Supplemental topographic data were obtained from the orbit I32 6-frame mosaic using a new, rapid, two-dimensional photoclinometry procedure developed by Paul Schenk, which takes the effects of local albedos into account. Although unreliable at 100-km wavelengths, these data provide detailed data for local relief such as scarps and ridges. For more information on these topographic datasets, see Schenk et al. (2004).

Table 1
Named volcanic and tectonic features in the Culann–Tohil region (refer to Fig. 1b)

Name	Lat (N)	Lon (W)	Size (km)	Hot spot	Notes	Origin of name
Michabo Patera[a]	1.7	167.1	100 × 58	Y	Detected by NIMS on orbit 31	Algonquin "great hare" & creator of the Earth, associated with the Sun & master of thunder & wind
Tsũi Goab Fluctus[a]	0.0	163.3	83 × 40	Y	Seen by NIMS, orbits 27, 31, 32	Khoi-Khoi (Hottentot) god of rain and thunder
Tsũi Goab Tholus[a]	0.5	162.4	56 × 35	N	Shield volcano east of Tsũi Goab Fluctus	Khoi-Khoi (Hottentot) god of rain and thunder
Culann Patera	−19.0	159.3	7 × 23 (vent)	Y	Detected by NIMS including on orbits 24, 32; Vent buried	Celtic smith god
Wabasso Patera[a]	−22.0	166.0	25	N		Potawatomi Sun god
Tohil Mons	−27.7	161.8	345.3 × 111.6[b]	N		Central American god who gave fire to man
Tohil Patera	−25.1	157.7	∼ 115 × 85[c]	N		Central American god who gave fire to man
Radegast Patera[a]	−26.9	159.2	29 × 21	Y	Detected by NIMS on orbit 32	Slav god of the Sun
Nina Patera	−37.2	161.9	Unknown	N	Vent buried	Inca god of fire

[a] Name provisionally approved by the IAU.
[b] From Schenk et al. (2001).
[c] From Turtle et al. (2001).

Table 2
Galileo mission encounters[a]

Mission	Flyby/orbit	Date
NOM	J0[b]	December 7, 1995
NOM	G1	June 29, 1996
NOM	G2	September 6, 1996
NOM	C3	November 6, 1996
NOM	E4	December 18, 1996
NOM	E5[b]	January 20, 1997
NOM	E6	February 20, 1997
NOM	G7	April 3, 1997
NOM	G8	May 7, 1997
NOM	C9	June 27, 1997
NOM	C10	September 18, 1997
NOM	E11	November 7, 1997
GEM	E12	December 16, 1997
GEM	E13[b]	February 10, 1998
GEM	E14	March 29, 1998
GEM	E15	May 31, 1998
GEM	E16[b]	July 21, 1998
GEM	E17	September 26, 1998
GEM	E18[b]	November 22, 1998
GEM	E19	February 1, 1999
GEM	C20	May 5, 1999
GEM	C21	June 30, 1999
GEM	C22	August 14, 1999
GEM	C23[b]	September 16, 1999
GEM	I24	October 11, 1999
GEM	I25	November 26, 1999
GEM	E26	January 4, 2000
GMM	I27	February 22, 2000
GMM	G28	May 20, 2000
GMM	G29	December 28, 2000
GMM	C30	May 25, 2001
GMM	I31	August 6, 2001
GMM	I32	October 16, 2001
GMM	I33	January 17, 2002
GMM	A34[b]	November 5, 2002
GMM	J35[b,c]	September 21, 2003

[a] Orbit letter designates primary remote sensing target: J, Jupiter; I, Io; E, Europa; G, Ganymede; C, Callisto; A, Amalthea. NOM, Galileo Nominal Mission; GEM, Galileo Europa Mission; GMM, Galileo Millennium Mission.
[b] No SSI data collected on these orbits.
[c] Galileo impact into Jupiter.

2.3. Galileo SSI color interpretation of Io

Io is the most colorful body in the Solar System, and the colors appear to represent volcanic materials with distinct compositions and/or emplacement styles. Thus, we attempted to utilize color to aid in our geologic mapping. Much new insight into the interpretation of Io's color pallette has been gained through study of Galileo SSI and NIMS data (e.g., Simonelli et al., 1997; Geissler et al., 1999, 2000), along with Hubble Space Telescope (HST: see Spencer et al., 2000) data and ongoing laboratory studies of volcanogenic sulfur (e.g., Kargel et al., 1999). Here we summarize concepts related to color interpretation of Io that are important for geologic mapping.

Because of the different geometries of the Galileo spacecraft's encounters with Io, color images of Io were obtained at a variety of resolutions and phase angles. Simonelli et al. (1997) and Geissler et al. (1999, 2000) discuss some of the complexities involved in assessing Io's color variations in terms of image geometry and photometry. Of key importance to geologic mapping is recognition that surface colors on Io change with increasing phase angle: polar deposits and some light-colored plume deposits around active volcanic centers brighten, whereas materials in the equatorial band darken (Geissler et al., 2000). These coloration changes were attributed to the presence of thin, fine-grained SO_2 frosts that are transparent under normal low-phase illumination but that become visible under high-phase illumination (Geissler et al., 2000). For consistency in geologic mapping, therefore, it is important to use color images that were obtained at a uniform, preferably low, phase angle. For all our color interpretation, we utilize the Galileo orbit C21 Io color mosaic of the antijovian hemisphere (July 1999), which was obtained at a phase angle of 4°.

A thorough summary of previous and current spectral and compositional interpretation of Galileo color data of Io was presented by Geissler et al. (1999). The Galileo SSI camera imaged Io at longer wavelengths than the Voyager camera, including a red filter at 665 nanometers (nm), and near-

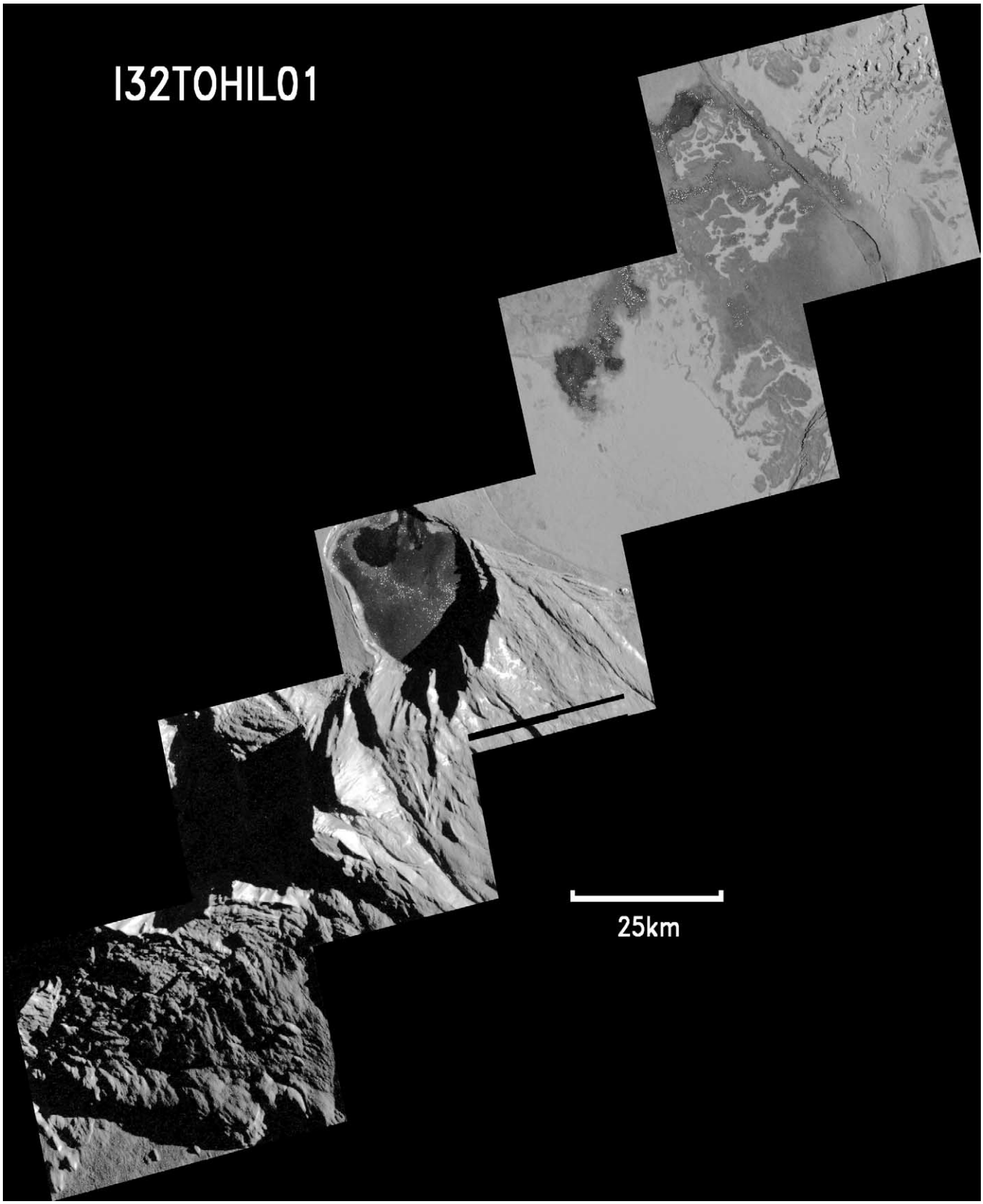

Fig. 3. Highest resolution (50 m/pixel) mosaic of a portion of the Culann–Tohil region of Io obtained by the Galileo spacecraft (NASA Planetary Photojournal Catalog Image #PIA03527.) This mosaic provides good views of the Mottled Mountain Material and Lineated Mountain Material on Tohil Mons, the Dark Patera Floor Material inside Radegast Patera, and the Bright Patera Floor Material in southwestern Tohil Patera. Image processing by David Williams, Arizona State University.

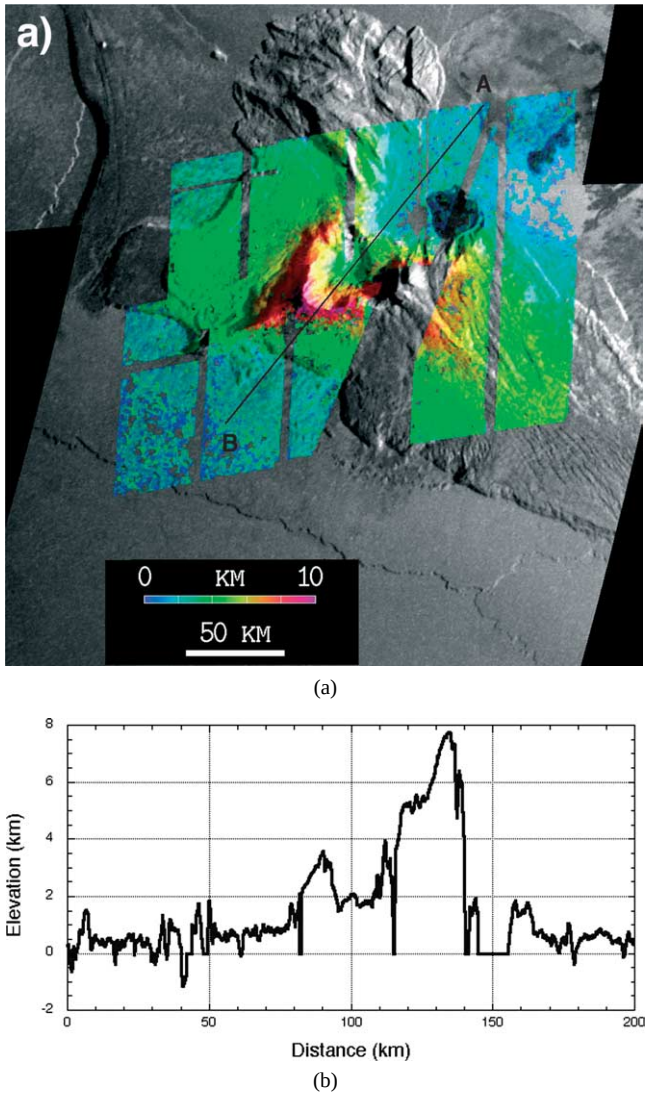

Fig. 4. (a) Digital Elevation Model (DEM) of Tohil Mons. The topography (color-coded according to the scale bar) was merged with low-sun medium resolution image mosaic of Tohil Mons from orbit I32. DEM was derived from analysis of I24–I27 stereo sequence and has a vertical precision of ∼ 50 m, although this is degraded slightly by the scrambling of the original I24 images (see Keszthelyi et al., 2001). The dark line shows the location of the profile in Fig. 4b. North is to the top. Image processing by Paul Schenk, Lunar and Planetary Institute. (b) Topographic profile across the center of Tohil Mons. The profile runs from north to south and shows the central depression of Tohil Mons, which lies ∼ 2 km above the surrounding plains and is surrounded by a low ridge to the north and a steep sided ridge to the southwest. Also apparent is a terrace block on the southern rim of the depression, which extends roughly half the circumference of the depression. Drop-outs are areas where the autocorrelation procedure failed to produce results.

infrared filters at 757, 888, and 991 nm. Combined with images obtained through the 413 nm (violet) and 560 nm (green) filters, the SSI produced color images of Io that are much closer to "true color" (i.e., that seen by the human eye) than any previous instrument (Figs. 1b, 2). Using available data from the SSI and NIMS, Geissler et al. (1999) defined four primary color units on Io: red materials, yellow materials, white materials, and dark materials. The red materials, which were subdivided into two subunits (regional red–orange units typically found in polar regions, and local red ring materials found around some active volcanic hotspots like Pele), are interpreted to be composed of short-chain sulfur molecules (S_3, S_4) resulting (in the case of the polar units) from breakdown of cyclo-S_8 by charged particle irradiation (Johnson, 1997) and (in the case of the red rings) by condensation from S_2-rich volcanic gases in the plumes of active vents (Spencer et al., 2000).

The yellow materials, which cover about 40% of Io's surface, were likewise subdivided by Geissler et al. (1999) into two subunits: regional yellow materials covering large equatorial plains, and local greenish-yellow patches observed near or in some paterae. Galileo SSI 4–6 point multispectral data were compared with the laboratory spectra of > 650 rocks and minerals, and Geissler et al. (1999) interpreted the yellow materials to be most consistent with cyclo-S_8 with or without a covering of SO_2 frosts deposited by plumes. Alternatively, Hapke (1989) showed that yellow color on Io can be produced by polysulfur oxide and S_2O without requiring large quantities of elemental sulfur, a hypothesis that is still viable. In contrast, the greenish-yellow patches are thought to be composed of either some sulfur compound contaminated by iron, or silicates such as olivine or pyroxene with or without sulfur-bearing contaminants. This interpretation is consistent with the locations of these units in or near paterae, suggesting intimate interaction between silicate lava

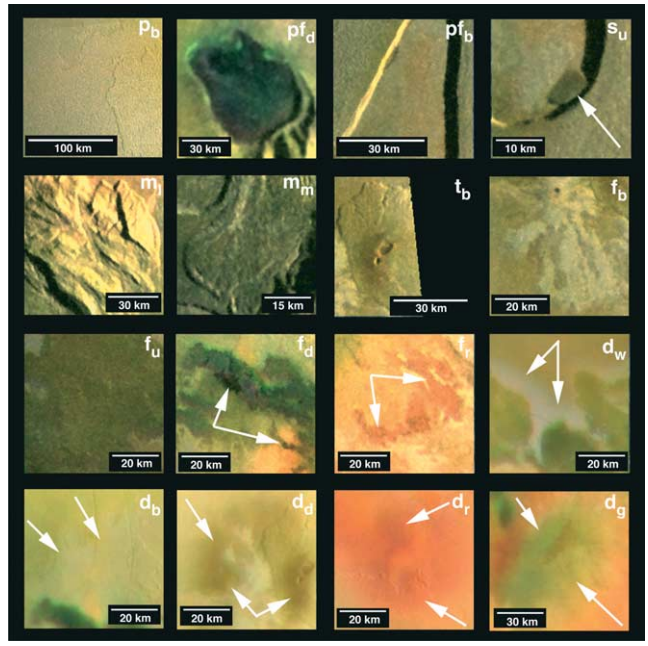

Fig. 5. Type examples of geologic units in the mapped area. Bright plains material, p_b; dark patera floor material, pf_d; bright patera floor material, pf_b; undivided slope material, s_u; lineated mountain material, m_l; mottled mountain material, m_m; bright tholus material, t_b; bright flow material, f_b; undivided flow material, f_u; dark flow material, f_d; red flow material, f_r; white diffuse material, d_w; bright diffuse material, d_b; dark diffuse material, d_d; red diffuse material, d_r; green diffuse material, d_g.

flows or lava lakes and either sulfur flows or sulfurous fallout from plumes (McEwen et al., 2000; Williams et al., 2000).

The white (to gray) materials cover about 27% of Io's surface, and have been extensively studied using NIMS data. The NIMS instrument has several detectors that are particularly sensitive to SO_2, whose data can be analyzed to assess grain size and abundance (e.g., Douté et al., 2001). The white units are interpreted to be composed of coarse- to moderate-grained SO_2 (Carlson et al., 1997), likely resulting from plume fallout that has recrystallized in Io's environment (Douté et al., 2001, 2002).

The dark spots, which cover about 1.4% of the surface, mostly correlate with active hotspots (Lopes-Gautier et al., 1999; Lopes et al., 2001). These spots occur as very dark (black) patera floors, lava flow fields, or as less-dark diffuse materials near or surrounding active vents. Galileo multispectral studies of the dark spots (Geissler et al., 1999) found that these materials were most consistent with Mg-rich orthopyroxene (enstatite or bronzitehypersthene), as indicated by their strong 0.9 μm absorption. Thus, these materials are interpreted to be composed of silicate lava flows or lava lakes (within paterae) or diffuse silicate pyroclastic deposits near paterae, of mafic to ultramafic composition (based on temperatures: see McEwen et al., 1998b).

It should be noted that the colors of some materials on Io change as they age. By aging, we refer to irradiation of surface materials, which tends to alter the color of sulfur materials (e.g., cyclo-S_8 develops metastable impurities S_3 and S_4, with colors ranging from brownish-yellow to grayish-yellow to orange: Nash and Fanale, 1977; Nelson and Hapke, 1978; Steudel et al., 1986; Hapke and Graham, 1989; Nelson et al., 1990). The red materials are very ephemeral at some vents, and tend to fade over a period of a few months. Dark materials tend to brighten with time, as they develop coatings of sulfurous materials from plume deposits (Nash et al., 1986). Bright materials tend to darken over time, as they interact with underlying or superposed materials. In addition to brightening and darkening, some color units can completely change, the best example of which is the red material on the floor of Pillan Patera which changed to a greenish color over several months (Phillips, 2000; Keszthelyi et al., 2001). Phillips (2000) interpreted this color change as due to a reaction of short-chain red sulfur (S_3, S_4) molecules with warm, dark silicate lava. Kargel et al. (1999) has reviewed the effects of various processes and interactions on sulfurous materials, and they indicate that color changes to sulfurous materials occur on timescales that are geologically important for Io (days to years). Therefore we think these type of surface changes may be useful in helping to determine relative ages at some localities.

3. Material units

Our initial analysis of the I32 image mosaic that serves as our basemap (Fig. 1b) revealed several features that were poorly discerned or indiscernable in the lower-resolution C21 color mosaic: the irregularly-shaped Michabo Patera, the new shield volcano Tsũi Goab Tholus, and the ambiguous mountain complex, Tohil. Tohil Mons is enigmatic in that it is adjacent to two apparently active paterae, both on the mountain's northeast flank. Closest to the mountain's flank is the smaller, almost circular ($\sim$ 28 km diameter) Radegast Patera. It has a dark floor and is a NIMS hot spot (Lopes et al., 2004), indicative of recent volcanism. Further to the northeast is the larger ($\sim$ 115 km $\times$ 85 km) Tohil Patera, which has a multicolored floor and more subdued topography. Most of the paterae in this region are elliptical or ovoid in shape, in contrast to several paterae in the Chaac–Camaxtli region that are irregularly-shaped and are thought to be indicative of some tectonic modification (Jaeger et al., 2001; Radebaugh et al., 2001; Williams et al., 2002). Previous studies of Io's mountains (Turtle et al., 2001; Schenk et al., 2001) indicate that Tohil Mons has a south-central massif that is $\sim$ 5–9 km tall, and has a WNW-ESE trend with a length of $\sim$ 345 km, a width of $\sim$ 111 km, and covers an area of $\sim$ 43,130 km^2. Our DEM confirms an elevation of $\sim$ 10 km at one isolated peak southeast of Radegast Patera. South of the Tohil mountain-patera complex is a pre-Voyager dark flow field named Mycenae Regio. It contains the apparently buried volcano Nina Patera, consists of a variety of ill-defined flows, and is surrounded by a halo of white diffuse material.

Our analysis of the Galileo images of the Culann–Tohil region suggests that there are at least 16 distinct morphologic units that can be identified, including 5 types of diffuse deposits. In all cases relative albedos and colors from the merged I32 mosaic were used, along with morphological differences, to define and characterize material units (unless otherwise specified). Although the colors of the Galileo images are typically more vibrant (particularly reds and blues) than the human eye would see (due to the SSI's filter wavelengths and the saturation caused by image processing that combines color with albedo and topography), they are a close approximation to the true color of Io's surface. Type localities of each material unit are shown in color in Fig. 5. Where possible, we have used map units developed from, or modified from, our previous work mapping the Chaac–Camaxtli region.

3.1. *Hummocky bright plains material,* p_b

Description: Layered, hummocky surface yellow to white–gray in color at equatorial latitudes to yellow–brown at polar latitudes, with albedo intermediate between Dark and Bright Patera Floor materials. Color images show some variation in the plains between darker and brighter areas, perhaps related in part to variations in SO_2 grain size or abundance (Douté et al., 2001). Plains near volcanic centers are mantled by various types of diffuse materials. Hummocky texture is somewhat variable, from ill-defined on the stratigraphically lowest layers to prominently ridged on the

stratigraphically highest layers, which tend to occur away from active volcanic centers. In the Culann–Tohil region the plains often contains scarps, grooves, pits, mesas, graben-like depressions, and channel-like features, in which scarp heights range typically from 50–100 m. No high-resolution grayscale images of the plains were obtained in this region, but near the eastern margin of Chaac Patera and Ot Mons individual hummocks were seen to be bright, irregular mounds in a matrix of darker, smoother material, oriented roughly N–S. (In the very high-res Chaac observation this is consistent with a roughly perpendicular orientation relative to the patera rim, but this pattern does not seem to hold across the lower resolution mosaic.) In this region, the ridged, mesa-like region between Tsũi Goab Tholus and Culann Patera has north–south trending ridges with amplitudes of 10 to 35 m (from photoclinometry) and spacings of 1–2 km.

Interpretation: Sulfur dioxide (SO_2)-rich surface shaped into periodic, km-scale undulations. Surface deposits formed by a combination of volcanic plume fallout (i.e., diffuse deposits near specific vents such as Prometheus and Culann) and frost deposition (i.e., frozen sulfurous gases from indeterminate sources that condense out of Io's atmosphere, covering wide areas). The process that forms the hummocky texture is not currently known, although some ideas include:

(a) rhythmic features produced by SO_2 sublimation,
(b) dunes deposited by pyroclastic activity (McEwen et al., 2000),
(c) tectonic modification of crustal materials (Moore et al., 2000),
(d) gravitational slumping (e.g., Moore et al., 2001),
(e) tidal working of light surface materials (e.g., Bart et al., 2004), or other presently unknown processes.

Orientations of the hummocks are shown to be consistent with current tidal flexing (Bart et al., 2004).

3.2. Dark Patera floor material, pf_d

Description: Reddish-green to gray to black surface with considerable variation in albedo and texture. In the high resolution (50 m/pixel) mosaic (Fig. 3) within Radegast Patera, this material appears smooth and dark (NIMS detected a warm spot in the small flow within Radegast Patera—see Lopes et al., 2004); higher-resolution images of the floor of Chaac Patera (Williams et al., 2002) showed that this material can contain an interwoven mixture of relatively bright and dark features, irregular hummocks, and pits. Usually little sulfur dioxide is present, based on previous studies using NIMS data (Lopes et al., 2001).

Interpretation: Green, red, brown, and gray surfaces are thought to be cool silicate lavas coated by sulfurous materials or various silicate and sulfurous flows; black surfaces are likely warm, recently-emplaced, coalesced silicate lava flows or (in cases where Dark Patera Floor Materials cover the whole interior of a patera) crusted lava lakes (Lopes et al., 2001; Douté et al., 2001; Radebaugh et al., 2004).

3.3. Bright patera floor material, pf_b

Description: Bright pinkish–white to red–orange to light gray unit with smooth surface at high and medium resolution. Has distinct contact with surrounding terrain, usually found within paterae but can also occur on or beyond their rims. Galileo NIMS data indicate an enhanced signature of sulfur dioxide in the pinkish-white material in southwestern Tohil Patera (Lopes et al., 2001), which SSI high-resolution images (Fig. 3) show to have flow-like margins.

Interpretation: White, yellow, and orange surfaces containing significant amounts of SO_2, requiring cold temperatures. Surfaces may be formed as coatings on cold silicate lava flows in inactive paterae (e.g., Michabo Patera), as primary flows or 'ponds' of sulfur or SO_2 (e.g., SW Tohil Patera), or as melting or sublimating Plains material being removed due to the heat of underlying, rising magma bodies (e.g., paterae in the Chaac–Camaxtli region: Keszthelyi et al., 2004).

3.4. Undifferentiated material, s_u

Description: Small, smooth, dark unit at the base of the southeast scarp inside Michabo Patera. This unit has a distinct contact with the patera floor, with highly linear margins and a top surface that appears to be angled away from the illumination direction. It is wider along its western margin than along the margin that is in contact with the inner patera wall. There are no lobes or other morphologic features clearly indicative of a lava flow, but there is also no indentation in the caldera wall to suggest collapse and no known landslide deposit on Io has a color different from its surroundings. The unit's linear margins might be more suggestive of a tectonic rather than volcanic origin. However, this unit may correlate with a new NIMS hotspot detected in the orbit I31 data (Lopes et al., 2004).

Interpretation: An unknown material, probably either a landslide or a lava flow. If a lava flow, the dark color suggests a silicate (mafic to ultramafic) composition.

3.5. Lineated mountain material, m_l

Description: Dark yellow to greenish-brown unit that appears cut by lineations in high-sun images, in which the lineations correspond to topographically-distinct ridges, grooves, graben, scarps, and lineaments in low-sun images. In Tohil Mons, a northern region (subunit 2) with more pronounced ridges and scarps (based on shadows) can be distinguished from a southern region with more subdued

ridges and scarps (subunit 1). This unit contains a steep-sloped amphitheater partially obscured by shadow. Parts of this unit may be mantled by bright diffuse material.

Interpretation: Sections of mountains disrupted by planar structural features. Structures are likely to be faults involved in uplift and/or lateral collapse of the edifice.

3.6. Mottled mountain material, m_m

Description: Dark yellow to greenish-brown unit that occurs in mottled lobes that are relatively lacking in lineations compared to the Lineated Mountain Material as seen in low-resolution, low-sun images. In high-resolution, low-sun images (Fig. 3), the mottled texture is seen to consist of domical mounds of material. In Tohil Mons, outlying regions of this material (subunit 1) appear more subdued and lack tall, sharp-edged scarps relative to the region that makes up the central mountain complex (subunit 2). Individual lobes of this unit contain a few scarps and ill-defined lineations, and individual domical mounds of this material occur below terminal scarps on the surrounding plains. Parts of this unit may be mantled by bright diffuse material.

Interpretation: Sections of mountains that show evidence of mass wasting processes, most likely involving flow with or without rotational sliding (e.g., debris aprons from rock and debris avalanches similar to those interpreted for Euboea Montes: Schenk and Bulmer, 1998). The older, degraded subunit 1 is interpreted to be a possible landslide, whereas the younger, fresher-appearing subunit 2 is interpreted to be a probable series of landslides.

3.7. Bright tholus material, t_b

Description: Yellow–brown unit that makes up an elliptical raised edifice ~ 40 by 55 km across that is separated from the surrounding plains by a distinct scarp, and which contains one or more circular central pits. Irregular radial grooves occur along the edges of the edifice. The edifice may be partially covered by dark diffuse material.

Interpretation: A shield volcano (Tsũi Goab Tholus) that may be largely composed of silicate or sulfurous materials (see discussion in Moore et al., 1986; Lopes et al., 2004).

3.8. Bright flow material, f_b

Description: At medium resolution, this unit appears as smooth bright yellow to orange–yellow sub-linear flows. Lengths exceed widths, but to a lesser extent than that observed in the dark flows in this region. The primary occurrence is just west of Tsũi Goab Tholus, in a region that corresponds to NIMS hot spot I27D (Lopes et al., 2001). These bright flows are generally less areally extensive than the dark flows in this region, and are less areally extensive than the bright flows in the Chaac–Camaxtli region. Contacts with surrounding terrain are distinct. Less distinct, less bright flows occur in Mycenae Regio.

Interpretation: Lava flows of sulfur-rich materials, or alternatively silicate flows covered by S-rich deposits. The bright flows of Tsũi Goab Fluctus may be the best example of active sulfur flows observed during the Galileo Mission. The darker colors in the Mycenae Regio bright flows may represent either variation in lava composition, variation in sulfurous coatings, or color change induced by radiation exposure (see Section 2.3).

3.9. Undivided flow material, f_u

Description: Terrain consisting of bright and dark flows with a range of albedos. Contacts are not distinct, making it difficult to distinguish individual flows.

Interpretation: Lava flows of indeterminate type, mostly likely from various Voyager-era or earlier sulfur-rich and/or silicate-rich effusive eruptions, older than materials defined as f_b, f_r, or f_d. Range of albedos due to coating of flow surfaces by pyroclastic materials or condensates, and/or the effects of aging in the ionian environment (see Section 2.3).

3.10. Dark flow material, f_d

Description: At medium resolution, appears as smooth dark (black to brown) lobate flows with lengths much greater than their widths. Contacts with surrounding terrain are sharp, and flows often extend toward and into apparent structural lows. Variation in albedos and cross-cutting relations can be used to define age relationships in some cases to separate younger (f_{d2}) from older (f_{d1}) flows. High-temperature hot spots usually correlate with dark flows as has been noted in NIMS observations (Lopes et al., 2001; Williams et al., 2002) both inside and outside paterae, including the small dark flow within Radegast Patera (Lopes et al., 2004). For example, the Culann Patera hot spot in I24 NIMS data appears to correlate with the source of the darkest flows at this volcano.

Interpretation: Lava flows of warm silicate materials from mafic or ultramafic silicate eruptions (see McEwen et al., 1998b; Williams et al., 2000). Range of albedos in dark flows due to variation in lava composition, coating of flow surfaces by sulfurous pyroclastic materials or condensates, or other effects of aging in the ionian environment.

3.11. Red flow material, f_r

Description: Red–brown irregular flow units with a distinct contact from surrounding material. This unit is so far unique to the Culann Patera volcanic complex. Comparison of the RGB color values of Diffuse Red Material, Dark Flow

Table 3
Typical RGB color values for several units in the Culann–Tohil region

Unit	Red	Green	Blue
Red flow materials	204	125	55
Dark flow materials	62	33	22
Red diffuse materials	202	96	40
Red-mantled dark flow materials	159	92	28

Note: Although the red flows are as red as the Red Diffuse Materials (and not as red as the red-mantled dark flows), they are much greener and bluer than either the dark flows or red-mantled dark flows, indicative of a different composition either intrinsic to the red flows or due to surface alteration.

Material, red-mantled dark flows, and Red Flow Material within Culann Patera (Table 3) suggests that this unit has a color distinct from that of the dark flows that are clearly mantled by red diffuse deposits. Although there must be some mantling of this unit by Red Diffuse Material, the color of this unit appears intrinsic to the unit itself. The areal extent of this unit is less than that of the Dark Flow Material in the Culann Patera volcanic complex.

Interpretation: Dark silicate lava flows which are compositionally different than those that constitute Dark Flow Material, although whether the difference is caused by surficial alteration or a distinct chemistry cannot be determined.

3.12. White diffuse material, d_w

Description: White unit that appears to thinly mantle underlying materials, occurring mostly as a halo around the flows of Mycenae Regio. This unit may also occur as a mantle that slightly obscures the texture in the Hummocky Bright Plains Material to the west and south of Michabo Patera; however, if present it is so thin that we cannot confidently map its boundaries and thus have not included it on the map.

Interpretation: Explosively-emplaced pyroclastic deposits, possibly dominated by sulfur dioxide. Volatiles may come from surficial deposits or near-surface 'aquifers' of SO_2 that are remobilized by nearby volcanic heat sources, as has been inferred to produce the radial white streaks around the Prometheus flow field (Kieffer et al., 2000; Milazzo et al., 2001).

3.13. Bright diffuse material, d_b

Description: Bright yellowish unit that appears to thinly mantle underlying materials, occurring mostly in an annulus surrounding Culann Patera (more clearly seen in global images).

Interpretation: Explosively-emplaced pyroclastic deposits dominated by sulfurous materials. SO_2 may be a component of this material; however, the color suggests that sulfur or other contaminants must be present.

3.14. Dark diffuse material, d_d

Description: Dark brown to black unit that appears to thinly mantle underlying materials, occurring mostly on Tsũi Goab Tholus and underlying the bright flows of Tsũi Goab Fluctus.

Interpretation: Explosively-emplaced pyroclastic deposits rich in mafic to ultramafic silicates, and possibly black sulfur in some cases. Spectral analysis of the dark diffuse deposit from the 1997 Pillan eruption is consistent with Mg-rich silicates (Geissler et al., 1999).

3.15. Red diffuse material, d_r

Description: Dark red unit that thinly mantles underlying materials, occurring as an asymmetric ring around Culann Patera with decreasing optical depth with increasing distance from the vent complex.

Interpretation: Explosively-emplaced pyroclastic deposits rich in metastable, short-chain sulfur polymers. The metastable S_3 and S_4 allotropes, red when quenched in their high-temperature forms (Spencer et al., 1997), could act as colorizing contaminants within bright, transparent material such as SO_2 (Geissler et al., 1999). Source appears to be primary magmatic S_2 gas (Smythe et al., 2000; Keszthelyi et al., 2001) coming from the Culann vent.

3.16. Green diffuse material, d_g

Description: Irregular, dark green unit that thinly mantles underlying materials, occurring primarily around the Culann vent complex inward of the Red Diffuse Material, but also as patches on the floor of Tohil Patera. The irregular boundaries appear to correspond with underlying dark flows.

Interpretation: Alteration coating produced by the interaction of Red Diffuse Deposits with warm silicate lava flows.

4. Galileo NIMS imaging of the Culann–Tohil region

Galileo NIMS obtained coverage over parts of the antijovian hemisphere at 1.0–4.7 μm during orbits I24–I27 and I31–I32, with various resolutions between ~ 500 m to 50 km/NIMS pixel. As previously stated, Lopes et al. (2001) identified two hot spots in the Culann–Tohil region in the NIMS data during orbits I24–I27. The first, located in Culann Patera, was detected numerous times during the Galileo mission and was classified as a persistent hot spot (Lopes-Gautier et al., 1999). It was detected as a bright hot spot during the orbit I24 flyby (color temperature $= 207 \pm 27\,^{\circ}\mathrm{C}$). Culann was also studied using NIMS to assess relative SO_2 abundance during orbit I25. Lopes et al. (2001) reported, building on their previous findings (Lopes-Gautier et al.,

2000), that a relatively high concentration of SO_2 corresponded to surfaces covered by reddish materials in the SSI images. As reddish diffuse deposits on Io were previously interpreted to be short-chain sulfur polymorphs (S_3–S_4) derived from cooled S_2 gas from explosive eruptions (Spencer et al., 2000; McEwen et al., 2000), and because pure SO_2 ice is thought to be transparent in visible light (appearing whitish) on Io, we interpret these results from Lopes et al. (2001) to suggest that some red deposits on Io may contain a contaminating SO_2 component, and that a mix of sulfur-bearing gases have been expelled from Culann during eruptions in the post-Voyager era.

Lopes et al. (2001) reported that the southwestern portion of Tohil Patera had an enhanced spectral signature for SO_2. We observe that this area corresponds to a section of the patera floor that is pinkish-white in color in recent SSI images, and that has the appearance of smooth, fresh bright flows with crenulated margins in the high-resolution Tohil mosaic (Fig. 3). We speculate that this material might be a series of SO_2 flows that flooded the southwestern floor of Tohil Patera. If so, then southwest Tohil Patera could be another example of 'ponds' of frozen SO_2 ice, perhaps effusively emplaced, as interpreted in Balder Patera by Smythe et al. (2000) and mapped by Williams et al. (2002).

A second hot spot in the Culann–Tohil region reported by Lopes et al. (2001) occurs west of Prometheus (labeled I27D in their Table 2), which has a blackbody temperature of $\sim 260 \pm 95$ °C. This temperature range falls within the range at which sulfur is a liquid (115–445 °C: Theilig, 1982). The hot spot appears to correspond with the apparently freshly bright flow field Tsũi Goab Fluctus, just west of the newly discovered shield volcano Tsũi Goab Tholus in the I32 mosaic (Fig. 1b). A review of lower-resolution color images from earlier Galileo flybys shows that bright flows were present in this location at least as early as orbit G2 (September 1996). Thus, any new bright flows emplaced from the visible I27D NIMS hot spot were of limited areal extent, and were superposed upon existing bright flows rather than covering additional plains. This hot spot was observed during the orbit I27 flyby (February 2000), but is not visible in the I31 (August 2001) and I32 (October 2001) NIMS data (the hot spots in these data are attributed to the dark material in Michabo Patera: Lopes et al., 2004). Although the measured NIMS temperature of I27D is also consistent with cooled silicate materials, the lack of any fresh dark materials in the area around the hotspot and the correspondence of the hotspot to a fresh-looking bright flow field suggest that Tsũi Goab Fluctus could be the best example of active effusive sulfur volcanism on Io during the Galileo mission. As stated, NIMS also detected warm spots in recent I31–I32 data that correlate with the darkest material within Radegast Patera, and with the dark spot within Michabo Patera, which are discussed more fully in Lopes et al. (2004).

5. Structures

Unlike the Chaac–Camaxtli region, the Culann–Tohil region contains a wide range of structural features, including scarps, ridges, grooves, pits, mesas, graben, and lineaments, that variously occur on Tohil Mons and in the equatorial plains. Several small, sub-circular depressions, which may be the remnants of inactive or undeveloped paterae, occur in the plains. From the north side of the Culann flow field extend several arcuate grooves, one of which terminates into a wider arcuate graben. These features may be the remnants of stress fractures in Io's crust resulting from tidal flexing, or perhaps nonsynchronous rotation. Michabo Patera could be a large collapse depression, as there is no evidence of volcanic features outside the depression. There are probably more structural features present than we have mapped, which were rendered invisible by extensive volcanic resurfacing.

Shadow lengths and directions reveal that most of the paterae in this region have depressed interiors, similar to terrestrial calderas. The shadow on the eastern edge of Michabo Patera corresponds to a depth of ~ 1.3 km. Tohil Patera, which has very little topographic expression (on the order of a few hundred meters from shadow measurements: Turtle et al., 2004), is an exception. The more prominent ridges on the north-central lobe of Lineated Mountain Material of Tohil Mons correspond to shadow heights of between 1–2 km.

As in all previous Io images, no impact craters were detected in this region, supporting the contention that Io's average surface is very young, perhaps a few million years old (McEwen et al., 2000).

6. Topography

While shadows can provide topographic information on individual features such as scarps, relative elevations of structures on regional scales must be derived from the C21–I24 stereo mapping coverage. Our mapping area occurs partially within Colchis Regio, an equatorial zone of relatively white smooth deposits punctuated by volcanic centers. Colchis Regio was thought to be broadly depressed 1–2 km relative to Io's tidally distorted ellipsoid (Gaskell et al., 1988; McEwen, 1995), based on Voyager low-resolution imaging. However, analyses of regional-scale stereo imaging of the Colchis Regio hemisphere (Schenk and Wilson, in preparation; Schenk and Wilson, 2003) suggests that the equatorial region centered on our mapping area is depressed no more than ~ 1 km relative to higher latitudes. Tohil Mons lies near the southern edge of this region.

Sites of individual volcanic eruptions in the mapping area appear to occur very close to the regional topographic norm. There appears to be little relief associated with Culann Patera, which lies at an elevation very similar to neighboring plains. The same appears to be true of Tsũi Goab Fluc-

tus, Wabasso Patera, Tohil Patera, and Mycenae Regio. The impression of relief on Tsũi Goab Tholus is confirmed by our photoclinometric mapping, which indicates relief on the order of 700 m from plains to crest (Schenk et al., in preparation). We note that this low shield volcano is capped by a small summit pit a few hundred meters deep. Within the plains themselves, as noted above, scarps are generally no more than 100 m high, as are the small pits and troughs due northwest of Culann Patera. With the exception of Tohil Mons, relief in our mapping area does not exceed 1 km.

Topographically, Tohil Mons can be divided into several major sections (Fig. 4). An elongate plateau roughly 180 by 115 km long forms the eastern half. This section roughly corresponds to our map unit m_{l1}. This plateau has a gently arching profile rising 3–5 km above the plains. The crest rises steadily from the eastern end to the western end near the center of the mountain, where it reaches a maximum height of ~ 8 km in the form of an isolated peak and where it is abruptly terminated by a scarp dropping down to the flat dark-floored Radegast Patera lying nearly at plains level. This plateau is divided in two sections along the crest, a somewhat smoother southern half and a northern part scored by several parallel graben-like valleys paralleling the topographic trend of the mountain and roughly 0.5 to ~ 1 km deep.

The western half of Tohil Mons consists of two major parts. The northern quarter (map unit m_{l2}) is a roughly circular plateau up to 6 km high crossed by deep graben-like valleys trending parallel to those in the eastern plateau. Several graben also crosscut these structures, however. The southern quarter (roughly, map units m_{m1} and m_{m2}) consists of several lobate shaped plateaus 1–2 km high, arranged in stepwise progression of increasing height.

Where the two halves of Tohil Mons are joined, two large amphitheaters are formed. The northern amphitheater is occupied by Radegast Patera. The southern amphitheater is roughly circular and sits 1.75 km above the northern amphitheater and is completely enclosed by a steep-sided scarp. The northern rim of this enclosed depression is ~ 2 km high above the surrounding plains, whereas the southern flank rises steeply at least 6 km high toward the main crest which rises ~ 11 km above the surrounding plains, and forms a circular arc surrounding the central depression. Along the southern scarp is a semicircular bench or terrace 3 km above the floor of the depression. This terrace is complete over only $1/4$ of the total circumference of the depression. A narrow linear ridge 3 to 6 km high extends southward from the main crest trending NW-SE further dividing Tohil Mons. Flow-like features along the flanks of these highs are tentatively interpreted as mass wasting features although a volcanic origin cannot be ruled out.

Based on these structural and topographic data, we suggest that Tohil Mons is consistent with formation by a combination of compressional uplift and surficial extension along the crest. The complex central morphology suggests involvement of two cross-cutting structural trends. Topographically, the western half could have moved laterally to the southwest, suggestive of strike-slip movement along the cross-cutting ridge, but there is little conclusive evidence for this hypothesis. The large enclosed central amphitheater could be volcanic in origin but no bright or dark volcanic deposits are discernable emanating from the depression or on its floor. The partial terrace on the southern wall is suggestive of partial failure of the depression walls, which could have buried the volcanic deposits, if any ever existed there. A concentration of intrusive activity is not unreasonable at the nexus of two intersecting structural trends but there is no indication that the construction of the Tohil Mons massif is volcanic in origin. If anything, volcanism is part of the degradational, rather than constructional, process of Tohil Mons.

7. Degradational processes

Landform degradation and mass wasting within the map area ranges from large multi-kilometer-scale mass movements to smaller, hectometer-scale scarp retreat. The scarp-like west and south faces of the Tohil Mons summit and the lobe-like material extending beyond and below the foot of that scarp are consistent with massive slope failure such as was reported for other ionian mountains such as Euboea Mons by Schenk and Bulmer (1998). These researchers interpreted the lobe-like material to be the result of large-scale rock and debris avalanches.

The crenulate bounding scarps of the large mesas and plateaus as well as the scarp at the base of Tsũi Goab Tholus could have formed by erosional retreat. This hectometer-scale scarp retreat might have been caused by one or more mechanisms, such as McCauley et al. (1979)-style SO_2 sapping or polysulfur oxide decomposition. Additionally, thermal erosion might have played a role; particularly in the scarp retreat of the mesas just north of Tohil Patera. Thermal erosion could have operated here if the mesas were composed of SO_2-rich material, perhaps a deposit of plume fallout, that later came under attack by high-temperature, low-viscosity lava flows which undercut the superjacent mesa material, analogous to a mechanism proposed for the erosional shaping of sinuous rilles on Mars and the Earth's Moon (e.g., Carr, 1974). The scarps may also be subject to plastic deformation and glacial-style flow of "warm" SO_2 interstitial ice (Moore et al., 2001).

8. Discussion and implications

We have synthesized the data discussed above to produce a geomorphologic map of the Culann–Tohil region, based on the Galileo SSI mosaic I32TERMIN01, including a stratigraphic correlation of the map units (Fig. 6). It is important to note that it is difficult to assess relative ages for some units, as we lack time marker horizons. Thus, all surfaces

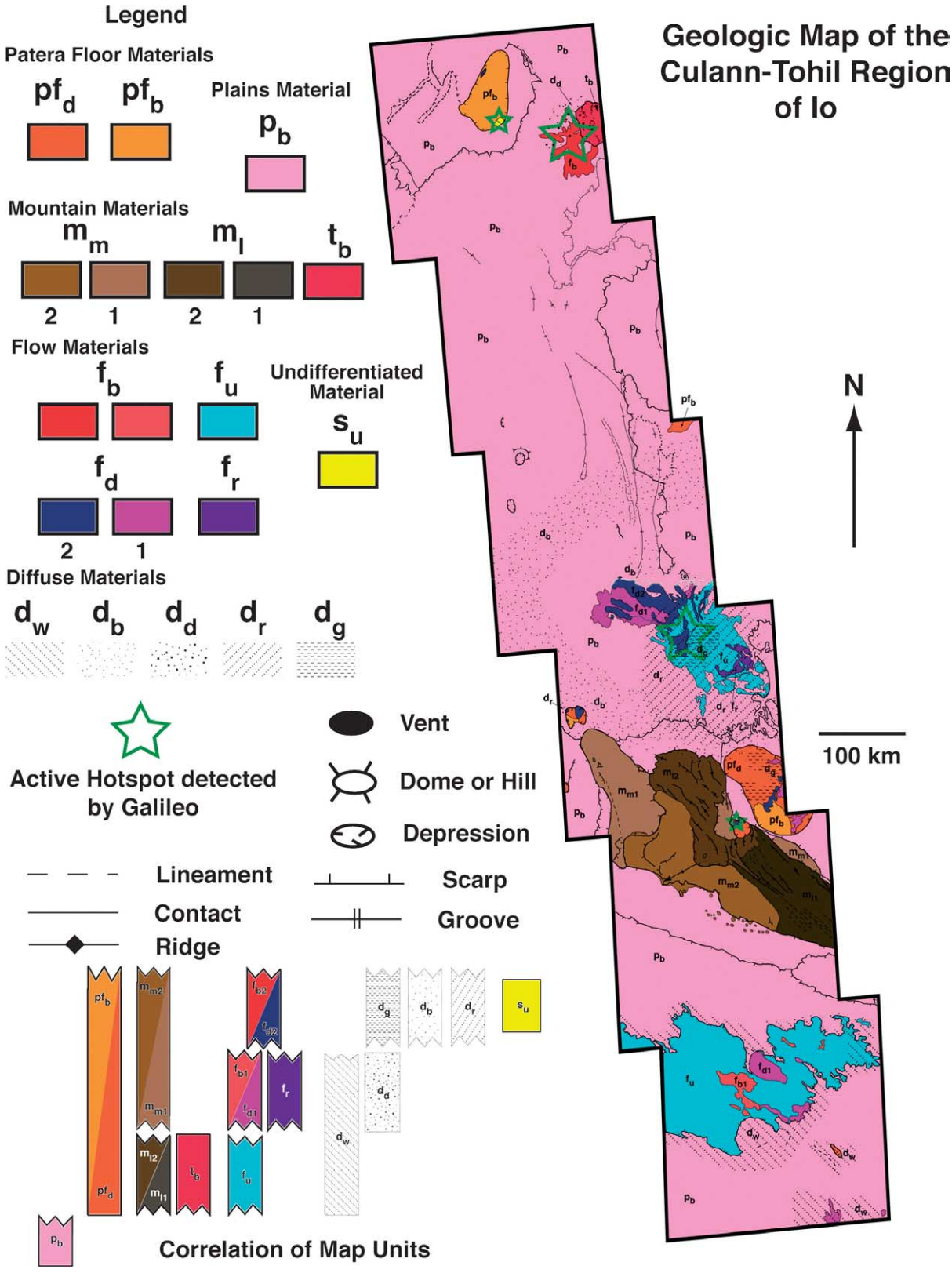

Fig. 6. Geomorphologic map of the Culann–Tohil region, including a stratigraphic correlation of map units. Based on Fig. 1b. Vent symbols refer to visible dark spots that appear to be the source of volcanic products. We assume most vents associated with active hotspots (green stars) inside paterae are buried by flow material. Dashed lines are used for contacts and structural features that are not as easily discerned in the image—they could be buried, or simply less well-exposed. For the stratigraphic correlation, it is important to note the difficulty in assessing relative ages for some units due to the lack of time marker horizons. Thus, the reader should be aware that all surfaces mapped as a given geologic unit may not have formed at the same time.

that are mapped as the same geologic unit did not necessarily form at the same time (as indicated by our stratigraphic correlation). In each of the following sections we discuss specific aspects of the geology of the Culann–Tohil region as inferred from our map and supporting data.

8.1. Changes since Voyager

In our previous paper (Williams et al., 2002), we discussed some of the problems involved in comparing Voyager and Galileo images, including variations in filter coverage (e.g., the Voyager Imaging Science Subsystem (ISS) camera did not image Io beyond orange wavelengths, whereas the Galileo SSI camera had both red and 756 nm filters, the latter of which was often used as our "red" component in RGB images), variations in resolution, and variations in lighting conditions (e.g., contrast reversals can occur with differences in phase angle). Thus, although it is difficult to make definitive statements about volcanically-induced surface changes, by using data from filters with comparable spectral range we have made several observations.

First, as in the Chaac–Camaxtli region (Williams et al., 2002), there is no evidence of large-scale (100s km) surface changes in this region over the last 23 years. All of the dark spots in the Voyager mosaic correspond to paterae and flucti that are resolved in Galileo images. Second, there are several small-scale changes that are apparent in the Culann–Tohil region. The greatest change occurs in and around Culann Patera: dark and bright flows observed by Voyager were buried either by recent bright explosive deposits or by dark lava flows (see also Keszthelyi et al., 2001). Fresh plume eruptions have produced the extensive diffuse deposits seen clearly even in global images. If there was any migration of the plume vent at Culann, as observed at Prometheus (McEwen et al., 1998a) and several paterae in the Chaac–Camaxtli region (Williams et al., 2002), it is below the resolution of the Voyager data (5–20 km/pixel). The freshest, darkest flows occur west of the presumed vent area, and are fed by one or more dark lava channels or tubes (Keszthelyi et al., 2001). The dark flows that occupied northwestern Tohil Patera in the Voyager images have mostly brightened, due in part to pyroclastic mantling from Culann. In contrast, Radegast Patera apparently has become darker, and thus volcanic activity closest to Tohil Mons appears to have shifted from Tohil Patera to Radegast Patera. Although the differences in image resolution between the Voyager flybys (5–20 km/pixel), the early Galileo flybys (2–10 km/pixel), the Galileo C21 flyby (1.4 km/pixel), and the Galileo I32 flyby (330 m/pixel) make it difficult to be certain, we think that some fresh bright flows were emplaced in Tsũi Goab Fluctus during the course of the Galileo Mission (see Section 4). Apparent brightening has occurred on the lava flows of Mycenae Regio, and some new bright and dark flows may have been emplaced since the Voyager flybys but prior to the Galileo flybys. However, it is interesting to note that the diffuse white halo around Mycenae Regio is apparently unchanged.

8.2. Volcanic features and eruption styles

If the assumption is made that most of the color variations on Io represent materials of different chemical composition, which to a first order appears to be the case (Geissler et al., 1999), then the visual evidence alone suggests that there is great volcanic diversity in this region, ranging from high-temperature, presumably silicate volcanism to low-temperature, presumably sulfur volcanism. Discrete, past geologic events can be recognized from the mapping and stratigraphic relationships (e.g., the dark diffuse deposit underlying bright flows at Tsũi Goab Fluctus, the dark undifferentiated unit in Michabo Patera). Recent bright, perhaps sulfur, flows were emplaced at Tsũi Goab Fluctus, whereas cryovolcanic sulfur dioxide was potentially emplaced as flows or as 'ponds' in SW Tohil Patera. Recent dark, probably silicate, flows were emplaced in Tohil and Radegast Paterae, and possibly two kinds of dark flows could have been emplaced at Culann Patera. There must be at least two volatile gases, S_2 and SO_2, that erupt either separately or in combination from Culann Patera to produce the different-colored, different-shaped rings of plume deposits, and one or more of these volatiles must make up the diffuse white halo around Mycenae Regio. The simplest explanation for this diversity of volcanic eruption styles and deposits is that there must be shallow reservoirs of liquid sulfur, liquid sulfur dioxide, and perhaps other sulfur-bearing materials that are tapped by rising silicate magmas, as first proposed by Kieffer (1982). Whether an eruption is explosive or effusive, or whether an eruption releases a product composed of sulfur, SO_2, silicate, or some combination of these materials, depends upon local environmental conditions (e.g., subsurface pressure), tectonic factors (e.g., degree and depth of subsurface fracturing of the crust), and magmatic conditions (i.e., chemical composition of rising silicate magmas and degree of interaction with various crustal volatile reservoirs). Indeed, Culann appears to be similar to Pele, which erupts both S_2 and SO_2 in its plumes (Spencer et al., 2000) and seems to have an intermittent plume that produces a red ring deposit, although at a much larger scale than Culann. Physical modeling by Cataldo et al. (2002) of the Pele and Pillan plumes supports the hypothesis that variation in gas content in rising silicate magma is the primary source for variation in explosivity and the dimensions of Io's plumes. It is unclear from the available data whether these volatiles are gases exsolved in ionian mafic to ultramafic magmas, or whether the magmas are "dry" and assimilate volatiles from crustal materials during ascent. Terrestrial ultramafic magmas are thought to have been quite effective at assimilating crustal materials (e.g., Huppert and Sparks, 1985; Williams et al., 1998). As was suggested for the bright flows in the Chaac–Camaxtli region (Williams et al., 2002), some of the bright flows in this region could represent sulfurous plains material

that was melted and remobilized by adjacent silicate magmas or lavas, as was inferred for the Mauna Loa sulfur flows (Greeley et al., 1984).

8.3. Bright plains formation

Although a definitive explanation for the genesis of Io's bright plains (and particularly, the formation of the hummocky texture) still eludes us, each new mapping exercise using Galileo data provides insights into the puzzle of bright plains formation. Williams et al. (2002) noted that inactive paterae in the Chaac–Camaxtli region have areas with the same basic color as the bright plains material but without the well-developed texture seen in the bright plains away from the paterae. They also suggested that as activity waned in paterae, sulfur-bearing plume materials were able to accumulate over time, burying patera floors and scarps and slowly transforming them into bright plains. Further support for this hypothesis is found in the Culann–Tohil region, where the apparently less active Michabo Patera may be in the early stages of this transformation. Alternatively or additionally, a new hypothesis by Keszthelyi et al. (this issue) suggests that paterae begin by sublimation of crustal volatiles resulting in the opening of caldera-like depressions which are eventually filled by dark silicate materials. It is clear that longer term study of paterae at high resolution and global mapping of paterae may be required to determine fully their evolutionary sequence.

The hummocky texture is variable across Io's plains. In this region, the bright plains are layered, and the texture is best preserved on mesas away from volcanic centers between Michabo and Culann Paterae. These layered plains are cut by irregular scarps, grooves, pits, graben, and channel-like features. Some of these features resemble those produced by erosional processes. There is no evidence of surface flows in this area, although there has certainly been mantling by plume deposits. Douté et al. (2002) suggested, from correlation maps of SO_2 abundance and granularity derived from Galileo NIMS data, that the equatorial plains seem to achieve some kind of steady state between condensation, metamorphism, and sublimation of SO_2 frost, and that SO_2 likely undergoes numerous cycles of sublimation/condensation at low latitudes. Moore et al. (2001) also suggested that sublimation degradation or decomposition of polysulfur oxides might play an important role in formation of Io's bright plains. We think one or more of these erosional processes must be responsible for at least some of the scarps, mesas, and channel-like features observed in the plains between Michabo and Culann Paterae.

8.4. Mountains and topographic relationships

Several SSI observations of the Galileo I32 flyby were selected to target Tohil Mons to better understand its structure and relationship to nearby paterae (Turtle et al., 2001 and 2004). Our image analyses, mapping, and studies of DEMs suggest that the mountain can be divided into a presumably older autochthonous portion, and a presumably younger displaced portion, in which the displacement was caused by mass wasting (e.g., flow with or without rotational sliding, such as landslides or debris avalanches). Such an interpretation is consistent with earlier studies of Io's mountains and other features affected by degradational processes (Schenk and Bulmer, 1998; Turtle et al., 2001; Moore et al., 2001). It is interesting to note that, despite the apparent migration of active high-temperature volcanism from Tohil Patera to Radegast Patera, it is the southwest side of Tohil Mons, the side that is apparently further from the active subsurface heat source, that has undergone the more significant mass wasting rather than the northeast side that is adjacent to Radegast Patera. Perhaps this fact is related to the compositional or structural nature of the crustal material that makes up Tohil Mons, or it is related to the orientation of the volcanic conduit that feeds Radegast Patera. Another possibility is that as materials from Tohil Mons slump into Radegast Patera, they are subsumed into the active lava lake, which quickly resurfaces itself, presenting us with a clean, chilled crust (Radebaugh et al., 2002). However, this possibility has not been rigorously assessed; it may be highly unlikely due to the volume of mountainous material involved. Furthermore, the direction and orientation of movement of the crustal blocks that make up Tohil remains unclear, although we think the western half could have moved laterally to the southwest, suggestive of strike-slip movement.

In contrast to the Chaac–Camaxtli region, there appears to be no relationship between volcanic activity and topography and structure in this region. The two active hotspots detected by NIMS (Culann Patera and Tsũi Goab Fluctus) occur in relative structural lows, as do the interiors of Wabasso, Radegast, and Tohil Paterae. However, these locations do not have substantially different relief from the surrounding plains. Michabo Patera, which appears to be less active, occurs on a mesa but also does not have substantially different relief from its surroundings.

The volcanic activity closest to Tohil Mons occurs in Radegast Patera, which we interpret to be the floor of a dark, mafic to ultramafic lava lake. If Io's crust is mostly mafic to ultramafic silicate covered in layers of sulfur-bearing compounds, then the lithosphere should have the strength to support mountains like Tohil Mons (Clow and Carr, 1980; Carr et al., 1998).

8.5. Subsurface relationships

We noted from mapping of the Chaac–Camaxtli region (Williams et al., 2002) that most of the active volcanic centers are associated with relative structural lows (as indicated by mapping of scarps), and that paterae on relative structural highs (i.e., mesas) tend to be less active or inactive. We assumed that structural highs and lows around individual features correlated with broader topographic highs and lows, such that active volcanism is being influenced by crustal

thickness: where the crust is thicker (topographic highs), dense mafic to ultramafic melts have a harder time erupting onto the patera floors and tend to produce deposits of limited areal extent and volume. In contrast, where the crust is thinner (topographic lows), dense magmas more easily erupt onto the surface, producing areally extensive dark flows with adjacent bright deposits of (presumably) sulfurous flows or plume deposits, likely from remobilized crustal sulfur-bearing sources (Williams et al., 2002). We did not have DEM analysis for our study of the Chaac–Camaxtli region, which we have utilized in this study, and which shows no correlation between location of active volcanism and surface relief (and presumably crustal thickness). We are currently preparing a DEM of the Chaac–Camaxtli region to better determine if there are any correlations between active volcanic sources and topography. It is clear that the relationships between locations of active volcanism and topography and crustal thickness are complex, and perhaps will require global geologic mapping and topographic analysis to elucidate these relationships.

9. Conclusions

Using Galileo SSI images from recent flybys (1999–2002: Keszthelyi et al., 2001; Turtle et al., 2004), along with NIMS spectral data processed for temperature estimates and compositional information (Douté et al., 2001, 2002; Lopes et al., 2001, 2004), we have produced a geomorphologic map of the Culann–Tohil region of Io's leading antijovian hemisphere. The Culann–Tohil region contains at least 8 volcanic centers, three of which were active hotspots within the last five years (Lopes et al., 2001, 2004). The most active volcano in this region is Culann Patera, which produces both lava flows and rings of plume deposits of different colors (and presumably different compositions), indicating a complex interaction between silicate magmas and shallow crustal reservoirs of sulfur and sulfur dioxide. We have mapped a new shield volcano Tsũi Goab Tholus, which has an adjacent bright flow field that is the source of a low-temperature NIMS hotspot, and may represent the best case for active effusive sulfur volcanism during the Galileo mission. The enigmatic mountain Tohil Mons is composed of an older unit of tectonically-disrupted, ridged-and-grooved crustal material, and a younger unit of displaced, mottled crustal material that was effected by mass movement. The two paterae neighboring Tohil Mons show evidence for volcanic resurfacing: Radegast Patera contains a dark, smooth floor interpreted to be a lava lake of mafic to ultramafic flows, whereas southwest Tohil Patera contains bright, SO_2-rich material with crenulated margins interpreted to be 'ponds' of SO_2 flows. The hummocky texture in the bright plains is best preserved on mesas north of Culann Patera, and the plains contain various features that may have been produced by erosional processes. There appears to be no correlation between the locations of the most active volcanic centers and surface topography, such that the role of crustal thickness variations in controlling volcanic ascent and eruption remains uncertain.

Acknowledgments

We thank Jennifer Blue of the US Geological Survey for assistance with the names approval process for the newly-identified features in our map region, and Lucas Kamp of JPL for assistance with the NIMS data analyses. This manuscript was substantially improved due to the comments of two anonymous reviewers. This research was supported by the National Aeronautics and Space Administration (NASA) under the Planetary Geology and Geophysics Program (PGG) Grant #NAG5-11787.

References

Bart, G., Turtle, E.P., Jaeger, W.L., Keszthelyi, L.P., Greenberg, R., 2004. Ridges and tidal stress on Io. Icarus 169, 111–127.

Carlson, R.W., Smythe, W.D., Lopes-Gautier, R.M.C., Davies, A.G., Camp, L.W., Mosher, J.A., Doderblom, L.A., Leader, F.E., Mehlman, R., Clark, R.N., Fanale, F.P., 1997. The distribution of sulfur dioxide and other infrared absorbers on the surface of Io. Geophys. Res. Lett. 24, 2479–2482.

Carr, M.H., 1974. The role of lava erosion in the formation of lunar rilles and martian channels. Icarus 22, 1–23.

Carr, M.H., McEwen, A.S., Howard, K.A., Chuang, F.C., Thomas, P., Schuster, P., Oberst, J., Neukum, G., Schubert, G., 1998. Mountains and calderas on Io: possible implications for lithosphere structure and magma generation. Icarus 135, 146–165.

Cataldo, E., Wilson, L., Lane, S., Gilbert, J., 2002. A model for large-scale volcanic plumes on Io: implications for eruption rates and interactions between magmas and near-surface volatiles. J. Geophys. Res. 107, 5109. doi:10.1029/2001JE001513.

Clow, G.D., Carr, M.H., 1980. Stability of sulfur slopes on Io. Icarus 44, 268–279.

Crown, D.A., Greeley, R., Craddock, R.A., Schaber, G.G., 1992. Geologic map of Io. US Geol. Surv. Misc. Invest. Series Map I-2209. 1 : 15,000,000, Reston, VA.

Douté, S., Schmitt, B., Lopes-Gautier, R., Carlson, R., Soderblom, L., Shirley, J., the Galileo NIMS Team, 2001. Mapping SO_2 frost on Io by the modeling of NIMS hyperspectral images. Icarus 149, 107–132.

Douté, S., Lopes, R., Kamp, L.W., Carlson, R., Schmidt, B., the Galileo NIMS Team, 2002. Dynamics and evolution of SO_2 gas condensation around Prometheus-like volcanic plumes on Io as seen by the Near Infrared Mapping Spectrometer. Icarus 158, 460–482.

Gaskell, R.W., Synnott, S.P., McEwen, A.S., Schaber, G.G., 1988. Large-scale topography on Io: implications for interal structure and heat transfer. Geophys. Res. Lett. 15, 581–584.

Geissler, P.E., McEwen, A.S., Keszthelyi, L., Lopes-Gautier, R., Granahan, J., Simonelli, D.P., 1999. Global color variations on Io. Icarus 140, 265–282.

Geissler, P., McEwen, A.S., Phillips, C., Simonelli, D., Lopes, R.M.C., Douté, S., 2000. Galileo imaging of SO_2 frosts on Io. J. Geophys. Res. 106, 33253–33266.

Greeley, R., Theilig, E., Christensen, P., 1984. The Mauna Loa sulfur flow as an analog to secondary sulfur flows (?) on Io. Icarus 60, 189–199.

Greeley, R., Spudis, P.D., Guest, J.E., 1988. Geologic map of the Ra Patera area of Io. US Geol. Surv. Misc. Invest. Series Map I-1949, 1 : 2,000,000, Reston, VA.

Hapke, B., 1989. The surface of Io: a new model. Icarus 79, 56–74.

Hapke, B., Graham, F., 1989. Spectral properties of condensed phases of disulfur monoxide, polysulfur oxide, and irradiated sulfur. Icarus 79, 47–55.

Huppert, H.E., Sparks, R.S.J., 1985. Cooling and contamination of mafic and ultramafic magmas during ascent through continental crust. Earth Planet. Sci. Lett. 74, 371–386.

Jaeger, W., Turtle, E.P., Keszthelyi, L.P., McEwen, A.S., 2001. Orogenic tectonism on Io. In: Proc. Lunar Planet. Sci. Conf. 32nd, Lunar and Planetary Institute, Houston. Abstract #2045 [CD-ROM].

Jaeger, W.L., Turtle, E.P., Keszthelyi, L.P., Radebaugh, J., McEwen, A.S., Pappalardo, R.T., 2003. Orogenic tectonism on Io. J. Geophys. Res. 108, 5093.

Johnson, R.E., 1997. Polar "caps" on Ganymede and Io revisited. Icarus 128, 448–469.

Kargel, J.S., Delmelle, P., Nash, D.B., 1999. Volcanogenic sulfur on Earth and Io: composition and spectroscopy. Icarus 142, 249–280.

Keszthelyi, L., Jaeger, W.L., Turtle, E.P., Milazzo, M., Radebaugh, J., 2004. A post-Galileo view of Io's interior. Icarus 169, 271–286.

Keszthelyi, L.P., McEwen, A.S., Phillips, C.B., Milazzo, M., Geissler, P.E., Williams, D.A., Turtle, E., Radebaugh, J., Simonelli, D., the Galileo SSI Team, 2001. Imaging of volcanic activity on Jupiter's moon Io by Galileo during GEM and GMM. J. Geophys. Res. 106, 33025–33052.

Kieffer, S.W., 1982. Dynamics and thermodynamics of volcanic eruptions: implications for the plumes on Io. In: Morrison, D. (Ed.), Satellites of Jupiter. Univ. of Arizona Press, Tucson, pp. 647–723.

Kieffer, S.W., Lopes-Gautier, R., McEwen, A.S., Smythe, W., Keszthelyi, L., Carlson, R., 2000. Prometheus: Io's wandering plume. Science 288, 1204–1208.

Lopes-Gautier, R., 13 colleagues, 1999. Active volcanism on Io: global distribution and variations in activity. Icarus 140, 243–264.

Lopes-Gautier, R., 15 colleagues, 2000. A close-up look at Io from Galileo's near-infrared mapping spectrometer. Science 288, 1201–1204.

Lopes, R.M.C., 14 colleagues, 2001. Io in the near infrared: NIMS results from the Galileo fly-bys in 1999 and 2000. J. Geophys. Res. 106, 33053–33078.

Lopes, R.M.C., 13 colleagues, 2004. Lava lakes on Io: observations of Io's volcanic activity from Galileo NIMS during the 2001 fly-bys. Icarus 169, 140–174.

McCauley, J.F., Smith, B.A., Soderblom, L.A., 1979. Erosional scarps on Io. Nature 280, 736–738.

McEwen, A.S., 1995. SO_2-rich equatorial basins and the epeirogeny of Io. Icarus 113, 415–422.

McEwen, A.S., 2002. Active volcanism on Io. Science 297, 2220–2221.

McEwen, A.S., 13 colleagues, 1998a. Active volcanism on Io as seen by Galileo SSI. Icarus 135, 181–219.

McEwen, A.S., 14 colleagues, 1998b. High-temperature silicate volcanism on Jupiter's moon Io. Science 281, 87–90.

McEwen, A.S., 25 colleagues, 2000. Galileo at Io: results from high-resolution imaging. Science 288, 1193–1198.

Milazzo, M.P., Keszthelyi, L.P., McEwen, A.S., 2001. Observations and initial modeling of lava-SO_2 interactions at Prometheus, Io. J. Geophys. Res. 106, 33121–33128.

Moore, H.J., 1987. Geologic map of the Maasaw Patera area of Io. US Geol. Surv. Misc. Invest. Series Map I-1851, 1 : 1,003,000, Reston, VA.

Moore, J.M., Wilhelms, D.E., 2001. Hellas as a possible site of ancient ice-covered lakes on Mars. Icarus 154, 258–276.

Moore, J.M., McEwen, A.S., Albin, E.F., Greeley, R., 1986. Topographic evidence for shield volcanism on Io. Icarus 67, 181–183.

Moore, J.M., Sullivan, R.J., Pappalardo, R.T., Turtle, E.P., the Galileo SSI Team, 2000. Degradation and deformation of scarps and slopes on Io: new results. In: Proc. Lunar Planet. Sci. Conf. 31st, Lunar and Planetary Institute, Houston. Abstract #1531 [CD-ROM].

Moore, J.M., Sullivan, R.J., Chuang, F.C., Head III, J.W., McEwen, A.S., Milazzo, M.P. , Nixon, B.E., Pappalardo, R.T., Schenk, P.M., Turtle, E.P., 2001. Landform degradation and slope processes on Io: the Galileo view. J. Geophys. Res. 106, 33223–33240.

Nash, D.B., Fanale, F.P., 1977. Io's surface composition based on reflectance spectra of sulfur/salt mixtures and proton-irradiation experiments. Icarus 31, 40–80.

Nash, D.B., Carr, M.H., Gradie, J., Hunten, D.M., Yoder, C.F., 1986. Io. In: Burns, J.A., Matthews, M.S. (Eds.), Satellites. Univ. of Arizona Press, Tucson, pp. 629–688.

Nelson, R.M., Hapke, B.W., 1978. Spectral reflectivities of the galilean satellites and Titan, 0.32 to 0.86 micrometers. Icarus 36, 304–329.

Nelson, R.M., Smythe, W.D., Hapke, B.W., Cohen, A.J., 1990. On the effect of X-rays on the color of elemental sulfur: implications for Jupiter's satellite Io. Icarus 85, 326–334.

Phillips, C.B., 2000. Voyager and Galileo views of volcanic resurfacing on Io and the search for geologic activity on Europa. PhD dissertation. Univ. of Arizona, Tucson, p. 269.

Radebaugh, J., Keszthelyi, L.P., McEwen, A.S., Turtle, E.P., Jaeger, W., Milazzo, M., 2001. Paterae on Io: a new type of volcanic caldera? J. Geophys. Res. 106, 33005–33020.

Radebaugh, J., McEwen, A.S., Milazzo, M., Davies, A.G., Keszthelyi, L.P., Geissler, P., Turtle, E.P., 2002. Lava Lakes in Io's Paterae. EOS Trans. AGU Spring Meet. Suppl. 83 (19). Abstract #P21B-06.

Radebaugh, J., McEwen, A.S., Milazzo, M.P., Keszthelyi, L.P., Davies, A.G., Turtle, E.P., Dawson, D.D., 2004. Observations and temperatures of Io's Pele Patera from Cassini and Galileo spacecraft images. Icarus 169, 65–89.

Schaber, G.G., Scott, D.H., Greeley, R., 1989. Geologic map of the Ruwa Patera quadrangle (Ji-2) of Io. US Geol. Surv. Geol. Invest. Series Map I-1980, 1 : 5,000,000, Reston, VA.

Schenk, P.M., Bulmer, M.H., 1998. Origin of mountains on Io by thrust faulting and large-scale mass movements. Science 279, 1514–1517.

Schenk, P., Hargitai, H., Wilson, R., McEwen, A.S., Thomas, P., 2001. The mountains of Io: global and geological perspectives from Voyager and Galileo. J. Geophys. Res. 106, 33201–33222.

Schenk, P.M., Wilson, R., 2003. Tectonic and regional topography of Io: a new high. In: Proc. Lunar Planet. Sci. Conf. 34th, Lunar and Planetary Institute, Houston. Abstract #2097 [CD-ROM].

Schenk, P.M., Wilson, R.R., Davies, A.G., 2004. Shield volcano topography and the rheology of lava flows on Io. Icarus 169, 98–110.

Shoemaker, E.M., Hackman, R.J., 1962. Stratigraphic basis for a lunar time scale. In: Kopal, Z., Mikhailov, Z.K. (Eds.), The Moon. Academic Press, London, pp. 289–300.

Simonelli, D.P., Veverka, J., McEwen, A.S., 1997. Io: Galileo evidence for major variations in regolith properties. Geophys. Res. Lett. 24, 2475–2478.

Smith, B.A., 21 colleagues, 1979a. The Jupiter system through the eyes of Voyager 1. Science 204, 951–972.

Smith, B.A., 21 colleagues, 1979b. The galilean satellites and Jupiter: Voyager 2 imaging science results. Science 206, 927–950.

Smythe, W.D., Lopes-Gautier, R., Douté, S., Kieffer, S.W., Carlson, R.W., Kamp, L., Leader, F.E., 2000. Evidence for massive sulfur dioxide deposit on Io. Bull. Am. Astron. Soc. 32 (3), 1047.

Spencer, J.R., McEwen, A.S., McGrath, M.A., Sartoretti, P., Nash, D.B., Noll, K.S., Gilmore, D., 1997. Volcanic resurfacing of Io: post-repair HST imaging. Icarus 127, 221–237.

Spencer, J.R., Jessup, K.L., McGrath, M.A., Ballester, G.E., Yelle, R., 2000. Discovery of gaseous S_2 in Io's Pele plume. Science 288, 1208–1210.

Steudel, R., Holdt, G., Young, A.T., 1986. On the colors of Jupiter's satellite Io: irradiation of solid sulfur at 77 K. J. Geophys. Res. 91, 4971–4977.

Tanaka, K.L., 11 colleagues, 1994. The Venus Geologic Mappers Handbook. USGS Open-File Rep. 94-438, p. 66.

Theilig, E., 1982. A primer on sulfur for the planetary geologist. NASA Contractor Rep. 3594, p. 34.

Turtle, E.P., 10 colleagues, 2001. The mountains of Io: global and geological perspectives from Voyager and Galileo. J. Geophys. Res. 106, 33175–33200.

Turtle, E.P., 14 colleagues, 2004. The final Galileo SSI observations of Io: orbits G28–I33. Icarus 169, 3–28.

Werner, A., 1964. African. In: MacCulloch, C.J.A. (Ed.). In: The Mythology of All Races, vol. VII. Cooper Square Publishers, New York, pp. 157–159.

Whitford-Stark, J.L., Mouginis-Mark, P.J., Head, J.W., 1991. Geologic map of the Lerna region (Ji-4) of Io. US Geol. Surv. Misc. Invest. Series Map I-2055, 1 : 5,000,000, Reston, VA.

Wilhelms, D.E., 1972. Geologic Mapping of the Second Planet. USGS Inter-Agency Rep., Astrogeology 55.

Wilhelms, D.E., 1990. Geologic mapping. In: Greeley, R., Batson, R.M. (Eds.), Planetary Mapping. Cambridge Univ. Press, Cambridge, UK, pp. 208–260.

Williams, D.A., Kerr, R.C., Lesher, C.M., 1998. Emplacement and erosion by Archean komatiite lava flows at Kambalda: revisited. J. Geophys. Res. 103, 27533–27549.

Williams, D.A., Wilson, A.H., Greeley, R., 2000. A komatiite analog to potential ultramafic materials on Io. J. Geophys. Res. 105, 1671–1684.

Williams, D.A., Radebaugh, J., Keszthelyi, L.P., McEwen, A.S., Lopes, R.M.C., Douté, S., Greeley, R., 2002. Geologic mapping of the Chaac–Camaxtli region of Io from Galileo imaging data. J. Geophys. Res. 107, 5068. doi:10.1029/2001JE001821.